A&A 531, A122 (2011)
DOI: 10.1051/0004-6361/201016287

Astronomy & Astrophysics

Diagnostics of the κ-distribution using Si III lines in the solar transition region

E. Dzifčáková[1] and A. Kulinová[1,2]

[1] Astronomical Institute Academy of Sciences of the Czech Republic, 251 65 Ondřejov, Czech Republic
e-mail: [elen;kulinova]@asu.cas.cz
[2] Department of Astronomy, Physics of the Earth and Meteorology, Faculty of Mathematics, Physics and Informatics, Comenius University, Mlynská dolina, 842 48 Bratislava, Slovakia
e-mail: kulinova@fmph.uniba.sk

Received 9 December 2010 / Accepted 11 May 2011

ABSTRACT

Aims. The solar transition region satisfies the conditions for appearance of the non-thermal κ-distribution. We aim to prove the occurrence of the non-thermal κ-distribution in the solar transition region and diagnose its parameters.
Methods. The intensity ratios of Si III lines observed by SUMER in 1100–1320 Å region do not correspond to the line ratios computed under the assumption of the Maxwellian electron distribution. We computed a set of synthetic Si III spectra for the electron κ-distributions with different values of the parameter κ. We had to include the radiation field in our calculations to explain the observed line ratios. We propose diagnostics of the parameter κ and other plasma parameters and analyze the effect of the different gradient of differential emission measures (DEM) on the presented calculations.
Results. The used line ratios are sensitive to T, density and the parameter κ. All these parameters were determined from the SUMER observations for the coronal hole (CH), quiet Sun (QS) and active region (AR) using our proposed diagnostics. A strong gradient of DEM influences the diagnosed parameters of plasma. The essential contributions to the total line intensities do not correspond to single T but a wider range of T, and they originate in different atmospheric layers. The amount of the contributions from these atmospheric layers depends on the gradient of DEM and the shape of the electron distribution function.
Conclusions. The κ-distribution is able to explain the observed Si III line spectrum in the transition region. The degree of non-thermality increases with the activity of the solar region, it is lower for CH and higher for the AR. The DEM influences the diagnosed T and N_e but it has only little effect on the diagnostics of the parameter κ.

Key words. Sun: transition region – Sun: UV-radiation

1. Introduction

A strong temperature or density gradient at low plasma densities in the solar transition region and corona can result in departures of the electron distribution function from the Maxwellian one. These electron distributions have an enhanced number of particles in the high-energy tail compared with the Maxwellian distribution. This kind of distribution can be described by the κ-distributions (e.g. Scudder & Olbert 1979a,b; Roussel-Dupré 1980; Shoub 1983; Scudder 1992; Ljepojevic & MacNiece 1988; Ljepojevic 1990; Vocks et al. 2008). The presence of the non-thermal electron distribution affects the ionization and excitation equilibrium and results in the changes of the relative intensities of spectral lines (Roussel-Dupré 1980; Dufton et al. 1984b; Dzifčáková 1992; Dzifčáková 1998; Dzifčáková 2005; Wannawichian et al. 2003).

Different ratios of the Si III emission lines from the transition region have been used previously for diagnostics of the plasma parameters. Dufton et al. (1983) have derived the electron densities from the Si III line ratios observed by *Skylab* and have reported the discrepancies in electron densities caused by enhanced intensity of the 1313 Å line. Dufton & Kingston (1989) have supposed the non-Maxwellian electron distribution of Shoub (1983) to explain the intensity of the 1313 Å line in data obtained with the high-resolution telescope and spectrograph onboard Spacelab 2. They found only partial agreement of the theory with the observations. Pinfield et al. (1999) have presented the observations of the Si III lines from SUMER, which show the enhancement in the intensity of the 1313 Å line, as well as some evidence of a small decrease in the temperature of ionization fraction, which changed from CH to AR. They have observed 10 lines of Si III in the spectral range 1100–1320 Å and proposed diagnostics of the plasma parameters from 11 line ratios to have a more complete analysis of the non-thermal effects in different solar regions. They concluded that the observed emission-line enhancement is evidence for the presence of a non-Maxwellian electron distribution in the transition region.

In this paper, we determine the parameters of the non-thermal electron distribution in the transition region and explain the observation of Pinfield et al. (1999). We assume that the non-thermal electron distribution in the transition region is a κ-distribution. Unlike other authors, we have included the influence of the radiation field on the excitation equilibrium of Si III in our calculations. The diagnostic method for the determination of N_e, T and the parameter κ of the κ-distribution is proposed, and the influences of DEM on the observed line ratios and diagnosed plasma parameters are discussed.

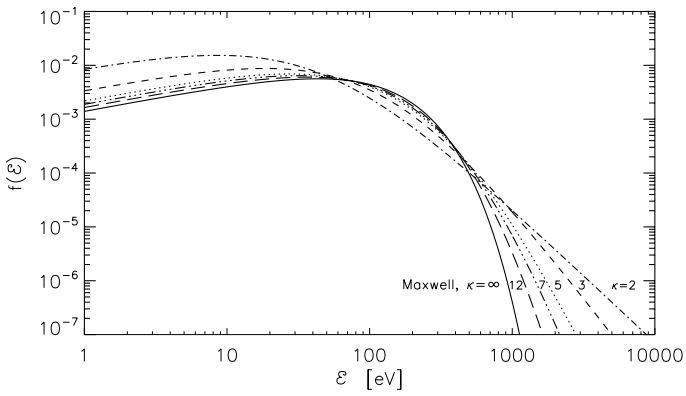

Fig. 1. Comparison of the Maxwellian distribution with the κ-distribution for κ = 12, 7, 5, 3, and 2.

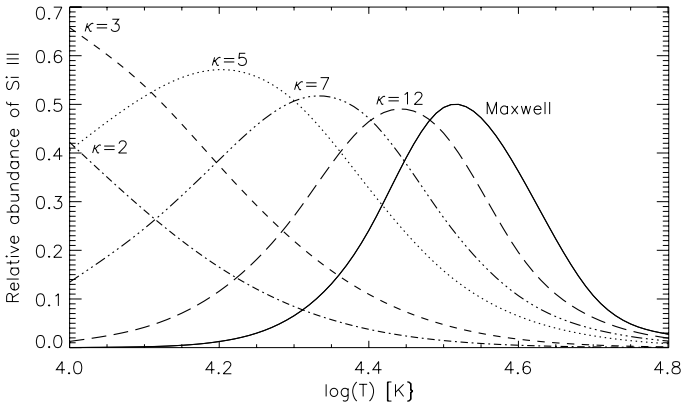

Fig. 2. Relative abundances of Si III for the Maxwellian distribution and the κ-distributions with κ = 12, 7, 5, 3, and 2.

2. Non-thermal electron distribution

The non-thermal electron κ-distribution with the enhanced number of particles in the high-energy tail is defined

$$f_\kappa(\mathcal{E})\mathrm{d}\mathcal{E} = \mathcal{A}_\kappa \frac{2}{\pi^{1/2}(kT)^{3/2}} \left(1 + \frac{\mathcal{E}}{(\kappa - 1.5)kT}\right)^{-(\kappa+1)} \mathcal{E}^{1/2}\mathrm{d}\mathcal{E}, \quad (1)$$

where $\mathcal{A}_\kappa = \Gamma(\kappa+1)/(\Gamma(\kappa-0.5)(\kappa-1.5)^{3/2})$ is the normalization constant, T is a parameter, and $\mathcal{E}$ is particle energy. The free parameter κ models the shape of the κ-distribution. It becomes a strong non-thermal distribution for $\kappa \to 1.5$ and is equal to the Maxwellian distribution for $\kappa \to \infty$ (Fig. 1).

The mean energy of the κ-distribution is $\langle\mathcal{E}\rangle = 3kT/2$ and pressure is $P = NkT$, where N is the density of particles. These expressions are the same as the relations for the Maxwellian distribution.

3. Ionization and excitation equilibrium

The ionization equilibrium for the κ-distributions has been calculated e.g. by Dzifčáková (1992), Dzifčáková (1998), Wannawichian et al. (2003). Figure 2 shows the changes in the abundance of Si III caused by κ-distribution as a function of $\log(T)$. Obviously, the dependence of the ion abundance on T is flatter, the abundance peak is wider and its maximum is shifted to a lower T value with increasing departure of the κ-distribution from the Maxwellian distribution. The shift of the abundance maximum of Si III is $\Delta\log(T) \simeq 0.15$ dex for the κ-distribution with κ = 12 and $\Delta\log(T) \simeq 0.35$ dex for κ = 7 compared with the maximum of the Si III abundance for the Maxwellian distribution at $\log(T/K) \simeq 4.6$.

The CHIANTI atomic database allows us to compute the line intensities for the Maxwell electron distribution (Landi et al. 2006). We used the original modification of CHIANTI software and database for the non-thermal κ-distributions. The modified software and extended database allow us to calculate the electron excitation rates, the excitation equilibrium and synthetic spectra under the assumption of κ-distributions (Dzifčáková 2006) by the method described in Dzifčáková & Mason (2008). Atomic data were taken from Dufton & Kingston (1989), Dufton et al. (1983), Martin et al. (1995), and Baluja & Hibber (1980). The 20-level model of Si III is included in CHIANTI 6.0 (Dere et al. 2009). Figure 3 shows a schematic diagram of the first 13 levels. The lines observed by SUMER are indicated.

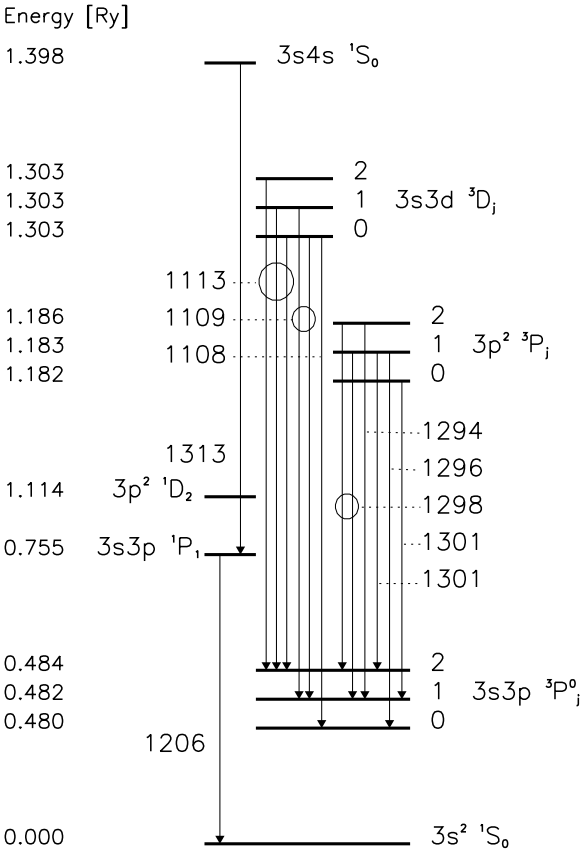

Fig. 3. Schematic diagram of the energy levels of Si III ion. The transitions of the observed emission lines are indicated.

The electron excitation rates for the non-thermal κ-distributions are a function of T and κ (Fig. 4). The κ-distributions can significantly increase the electron excitation rates for high ratios of $\Delta E/kT$, where ΔE is excitation energy. The enhancement of the electron excitation rates can be several orders for low T and this enhancement increases with the increase of the transition excitation energy. However, the details depend on the type of the transition and on the behavior of the cross-section with incident electron energy. On the other hand, the electron excitation rates are lower than for a Maxwellian distribution for the transitions with low excitation energies and for higher T. Evidently, κ-distributions significantly affect all transitions. The effect is higher for transitions with higher excitation energy (Fig. 4 *left* and *middle*) and similar changes

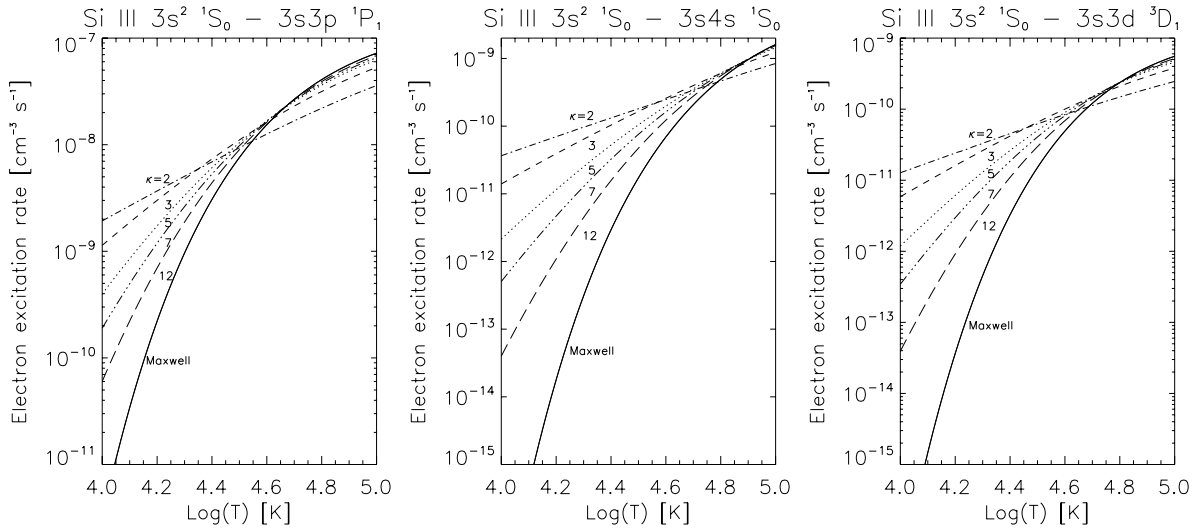

Fig. 4. Dependence of the electron excitation rates on T for Maxwellian distribution and the κ-distributions with κ = 12, 7, 5, 3, and 2 for three different transition, $3s^2\,^1S_0$–$3s4s\,^1S_0$ with ΔE = 0.480 Ry (*left*), $3s^2\,^1S_0$–$3s3p\,^1P_1$ with ΔE = 1.450 Ry (*middle*), and $3s^2\,^1S_0$–$3s3d\,^3D_1$ with ΔE = 1.303 Ry (*right*).

Table 1. List of the used lines.

λ	Transitions
1108	$3s3d\,^3D_1$–$3s3p\,^3P_0$
1109	($3s3d\,^3D_1$–$3s3p\,^3P_1$) + ($3s3d\,^3D_2$–$3s3p\,^3P_1$)
1113	($3s3d\,^3D_1$–$3s3p\,^3P_2$) + ($3s3d\,^3D_2$–$3s3p\,^3P_2$) + ($3s3d\,^3D_3$–$3s3p\,^3P_2$)
1206	$3s3p\,^1P_1$–$3s^2\,^1S_0$
1294	$3p^2\,^3P_2$–$3s3p\,^3P_1$
1296	$3p^2\,^3P_1$–$3s3p\,^3P_0$
1298	($3p^2\,^3P_2$–$3s3p\,^3P_2$) + ($3p^2\,^3P_1$–$3s3p\,^3P_1$)
1301	$3p^2\,^3P_0$–$3s3p\,^3P_1$
1313	$3s4s\,^1S_0$–$3s3p\,^1P_1$

can be observed for transitions with a similar excitation energy of the upper level (Fig. 4 *middle* and *right*). The electron excitation rates for the κ-distributions lead to changes in the populations of each of the energy levels compared with the thermal case.

The level populations and line intensities are influenced by the electron density, the electron excitation and de-excitation rates as well as the radiative transitions, and are the result of the excitation equilibrium. A grid of model spectra was computed for κ-distribution with κ = 2–34 and Maxwellian distribution. T was taken from the interval 10^4 K–10^5 K and densities from 10^8–10^{12} cm^{-3}. We assumed a radiation field with $T_{\rm rad}$ = 6000 K and a height h = 1.003 $R_\odot$ (2.5 Mm). We tried different heights in the range 1.0–1.05 $R_\odot$, however, the variation in the results were minimal.

4. Diagnostics

Table 1 summarizes the Si III lines used for the diagnostics. Their ratios are labeled R1–R11 and are listed in Table 2.

If no contribution of the radiation field is considered, the R1–R6 ratios are almost insensitive to T and R7–R11 to $N_{\rm e}$ for the Maxwellian distribution (Pinfield et al. 1999). This is valid neither for the Maxwellian nor for the κ-distribution when the radiation field is included.

For diagnostic purposes we used the same line ratios as Pinfield et al. (1999) but we included the radiation field. A comparison of our T–$N_{\rm e}$ plots for the Maxwellian distribution with

Table 2. List of the line ratios.

Ratio	λ_1(Å)/λ_2(Å)	Ratio	λ_1(Å)/λ_2(Å)
$R1$	1108/1294	$R7$	1301/1296
$R2$	1108/1296	$R8$	1301/1298
$R3$	1108/1298	$R9$	1313/1113
$R4$	1109/1296	$R10$	1294/1206
$R5$	1113/1294	$R11$	1296/1206
$R6$	1113/1298		

and without radiation field is given in Fig. 5. The differences in the diagrams are significant, mainly for low T and lower $N_{\rm e}$. Some of our plots with the included radiation field involve points for which two values of T and $N_{\rm e}$ are possible.

The observed line ratios are marked by crosses with their error bars in Fig. 5. The values of T and $N_{\rm e}$ obtained for CH and QS in both columns lie in the range of acceptable values, however, they differ significantly from each other. For AR, the cross lies outside of the diagram (Fig. 5 *right top*). Apparently, the Maxwellian distribution is not able to explain the observations.

To move from the thermal to the non-thermal distribution, we need to diagnose three parameters simultaneously. It is not possible to do this in a single diagram. We used a numeric method to diagnose κ. This method uses our grid of the calculated values of R1–R11 for different T, $N_{\rm e}$, and κ and looks for a minimum in the difference between the observed and theoretical line ratios. The results of these diagnostics and their comparison

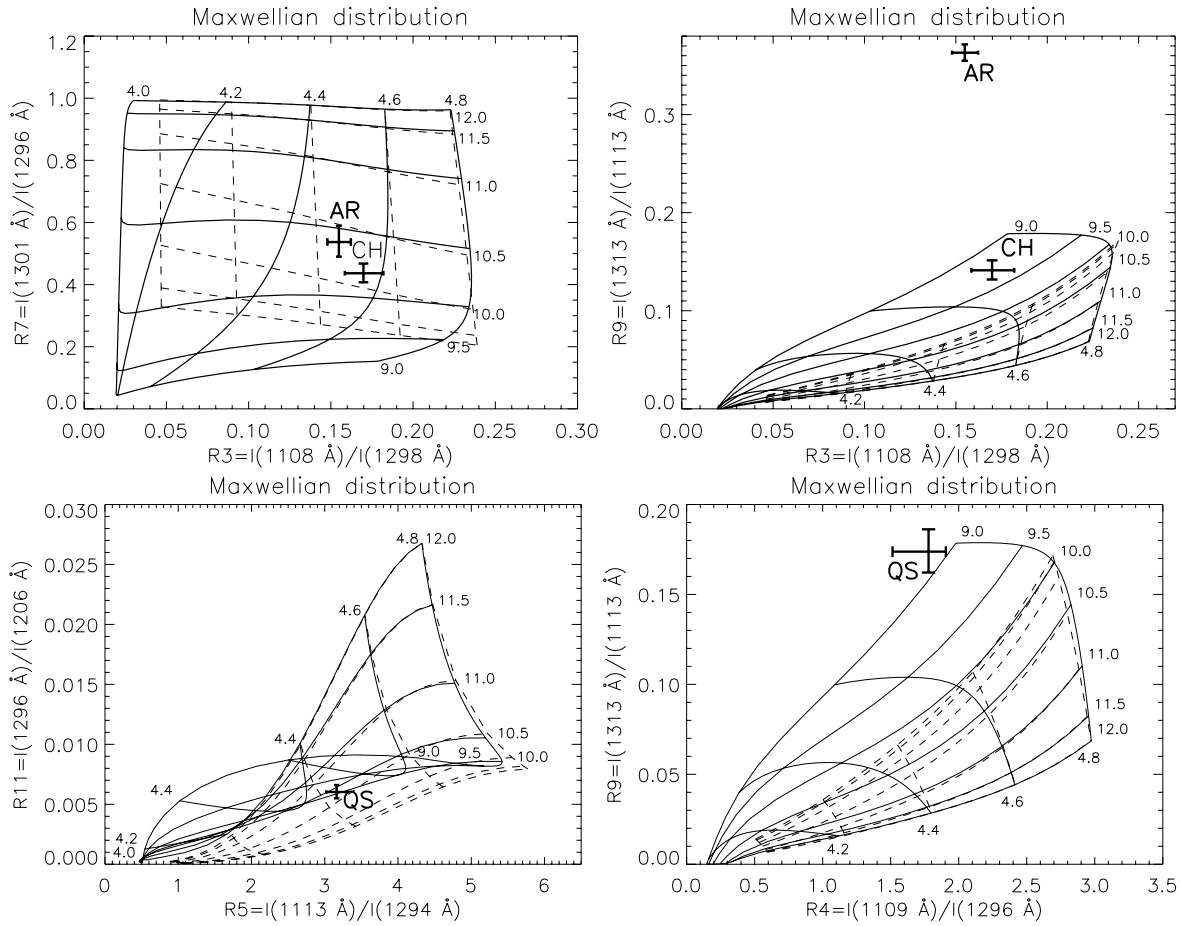

Fig. 5. Schematic T–N_e diagnostic diagrams for Maxwellian distribution with (full lines) and without (dashed lines) included radiation field for AR and CH (*top*) and for QS (*bottom*). The crosses show the observed values for AR, QS, and CH with their errors by Pinfield et al. (1999).

with thermal diagnostics are given in Table 3. They agree with the observed line ratios within their errors and we can consider this agreement as evidence of the presence of the κ-distributions or distributions with a very similar shape in the transition region. Figure 6 shows several diagrams with the observed line ratios for diagnosed values of κ.

5. Diagnosed plasma parameters and discussion

The diagnosed κ for QS (κ = 12–9) is only slightly lower than the κ for CH (κ = 13–12) and indicate a similar degree of non-thermality. The active region shows the strongest deviation from the Maxwellian distribution with κ = 7. As has been predicted by Scudder (1992), the suprathermal tail of the distribution is enhanced above locations with the intensified magnetic field. Scudder (1992) has estimated the value of $\kappa \approx 2.2$ for the transition region. On the other hand, MacNeice et al. (1991) have calculated the non-Maxwellian effects in the transition region and concluded that only weak departures from Maxwellian distribution can occur, so κ should be high. Our diagnosed values of κ lie between these two extrema. The values of κ in CH and QS correspond to smaller departures from the Maxwellian distribution. The diagnosed value of κ = 7 in the AR is slightly higher than κ = 2–5.5 diagnosed in the solar wind (e.g. Maksimovic et al. 1997; Nieves-Chinchilla & Viñas 2008; Zouganelis 2008; Pierrard & Lazar 2010). However, our diagnosed values of κ can be influenced by data averaging over the observed region.

The values of T and N_e correspond to the typical parameters of plasma at the base of the transition regio, however, T diagnosed for AR appears to be too low. Previously, authors used different pairs of the Si III lines for diagnostics of the electron density in the transition region than those proposed by Pinfield et al. (1999). They assumed the Maxwellian distribution, although they did not include the influence of the radiation field on the diagnostics and they did not diagnose T, therefore, they had to assume its value. Dufton et al. (1983) have derived the range of the electron densities under the assumption of two values of $\log(T/\mathrm{K})$ = 4.5 and 4.7 as $\log(N_e/\mathrm{cm}^{-3})$ = 9.0–10.4 for CH, $\log(N_e/\mathrm{cm}^{-3})$ = 9.0–10.3 for QS, and $\log(N_e/\mathrm{cm}^{-3})$ = 8.8–11.3 for AR. Similar results have been derived by Keenan et al. (1989a) and Doschek et al. (1998). Keenan et al. (1989b) have used the Shoub's non-thermal model of the transition region and for the assumed $\log(T/\mathrm{K})$ = 4.5 or 4.7 presented $\log(N_e/\mathrm{cm}^{-3})$ = 10.2–10.8 for a quiet region and $\log(N_e/\mathrm{cm}^{-3})$ = 10.4–11.0 for AR.

Generally, the electron densities derived from Si III lines agree with the values derived from lines of the other ions. For example, Pérez et al. (1999) have studied a temporal variability in the electron density from O IV lines. They have found that $\log(N_e/\mathrm{cm}^{-3}) = 9.7$–$10.4$ with a maximum at ≈9.7 in CH, $\log(N_e/\mathrm{cm}^{-3}) = 9.7$–$10.8$ with a maximum at ≈9.8 in QS, and $\log(N_e/\mathrm{cm}^{-3})$ = 9.7–11.0 with a maximum at ≈10.5 in AR. The amplitude of the temporal and spatial changes has reached $\Delta\log(N_e/\mathrm{cm}^{-3}) \approx 0.5$ dex.

Table 3. Summary of the diagnosed T, N_e and κ, together with the corresponding synthetic values of the ratios R1–R11. x.

Coronal hole								
log(T)	log(N_e)		R1	R2	R3	R7	R8	R9
4.55	10.3	Maxw.	0.60	0.75	0.17	0.48	0.11	0.08
4.40	10.15	$\kappa = 13$	0.61	0.75	0.17	0.46	0.10	0.14
4.40	10.15	$\kappa = 14$	0.60	0.73	0.17	0.45	0.11	0.14
Observed ratio			0.59 ± 0.04	0.71 ± 0.05	0.17 ± 0.02	0.44 ± 0.03	0.11 ± 0.005	0.14 ± 0.01
Quiet Sun								
log(T)	log(N_e)		R4	R5	R6	R9	R10	R11
4.50	10.0	Maxw.	1.59	3.28	0.92	0.08	0.0076	0.0061
4.55	9.25	$\kappa = 12$	1.53	3.23	0.90	0.16	0.0078	0.0063
4.55	9.25	$\kappa = 11$	1.57	3.29	0.92	0.17	0.0077	0.0062
4.55	9.2	$\kappa = 10$	1.54	3.23	0.90	0.17	0.0077	0.0062
4.55	9.2	$\kappa = 9$	1.60	3.31	0.93	0.19	0.0075	0.0061
Observed ratio			1.70 ± 0.2	3.16 ± 0.15	0.91 ± 0.05	0.17 ± 0.02	0.0078 ± 0.0004	0.0060 ± 0.0006
Active region								
log(T)	log(N_e)		R2	R3	R4	R7	R8	R9
4.50	10.4	Maxw.	0.67	0.16	1.81	0.53	0.12	0.07
4.00	10.1	$\kappa = 7$	0.69	0.16	1.99	0.49	0.11	0.34
Observed ratio			0.66 ± 0.03	0.16 ± 0.01	1.66 ± 0.08	0.54 ± 0.05	0.13 ± 0.01	0.36 ± 0.01

Notes. The observed values with their errors are listed as well.

Our results for the electron density in CH (Table 3) agree with the previous authors. The log(T) for diagnosed κ = 13–14 is lower than for the Maxwellian distribution. This is beacause of a shift of the ionization peak of Si III to lower T (Fig. 2).

The diagnosed electron density for QS (Table 3) appears to be lower than for CH. When we exclude data errors, there are three possible explanations:

- The intensity of the 1206 Å line in the R10 and R11 ratios can be influenced by its own opacity (e.g. Keenan & Kingston 1986), resulting in higher values of both ratios. Figure 6 shows that a lower ratio of R11 implies a higher electron density.
- The inhomogeneity of the analyzed quiet region can lead to incorrect results. The He II figure of the quiet region in Pinfield et al. (1999) shows bright and dark features, which must have different plasma parameters.The data of Pinfield et al. (1999) used here are the line intensities averaged over the whole region.
- The effect of the DEM. The line intensities are integrated along line of sight through the region with a strong gradient of the electron density and T. The effect of DEM on the ratios of the line intensities can be much stronger for the κ-distributions than for the Maxwellian distribution. This is because the κ-distribution broadens the ionization peak and increases electron excitation rates for the lower T compared with the Maxwellian distribution. Therefore, the layers from a much wider interval of T contribute to the integral intensity along the line of sight for the κ-distribution.

The diagnosed N_e for AR (Table 3) agrees with the generally accepted densities for AR in the transition region. However, the diagnosed value of T is quite low. We must note that T in the κ-distribution represents the mean energy of the distribution. The ionization and excitation state for a particular mean energy of electrons in a κ-distribution is similar to the ionization and excitation state for the Maxwellian distribution with a higher mean energy. This is owing the the enhanced number of electrons in the high-energy tail of the κ-distribution. The possible explanation for log(T/K) = 4.0 diagnosed in AR could be the shift of the ionization peak due to the κ-distribution. The shift for κ = 7 is about 0.35 dex toward lower T, but the diagnosed shift is 0.5–0.6 dex. Thus, the shift of the ionization peak alone cannot explain the diagnosed log(T). We assume that this large shift is caused by the gradient of the density in the transition region and could be explained by an appropriate DEM.

6. Effect of DEM

The transition region is characterized by strong gradients of the electron density and temperature. The deeper and colder layers with higher densities can have more important contributions to the observed line intensity than hotter layers with lower densities. We do not know the real DEM for the observed regions, and there are no DEM computed under the assumption of the non-thermal distribution. This is why we choose the DEMs for the Maxwellian distribution from CHIANTI, purely to illustrate a possible effect of DEM on the line intensities. Three different DEMs by Vernazza & Reeves (1978) for the quiet Sun (DEM 1), a coronal hole (DEM 2), and the active region (DEM 3) were taken from the CHIANTI database (Fig. 7) to test an effect of the integration of the line emission along the line of sight on the diagnostics. The DEM 3 has the strongest gradient and DEM 1 has the lowest one (Fig. 7).

The intensity of the optically thin line formed in an atmosphere with a DEM is (e.g. Philips et al. 2008)

$$\begin{aligned} I_\lambda &= \frac{hc}{4\pi\lambda_{\rm ji}} A_{ji} \int N(\mathrm{X}_j^{+k})\,\mathrm{d}l \\ &= \frac{hc}{4\pi\lambda_{ij}} A_{ji} \int \frac{N(\mathrm{X}_j^{+k})}{N(\mathrm{X}^{+k})} \frac{N(\mathrm{X}^{+k})}{N(\mathrm{X})} \frac{N(\mathrm{X})}{N(\mathrm{H})} \frac{N(\mathrm{H})}{N_e} N_e \mathrm{d}l \\ &= \frac{1}{4\pi} \int G(T, N_e) N_e^2\,\mathrm{d}l \\ &= \frac{1}{4\pi} \int G(T, N_e)\,\mathrm{DEM}\,\frac{T}{\log(e)} \mathrm{d}\log(T), \end{aligned} \tag{2}$$

where $G(T, N_e)$ is the contribution function, DEM = $N_e^2 \mathrm{d}l/\mathrm{d}T$ is the differential emission measure, λ_{ji} is wavelength of the spectral line, A_{ji} is the Einstein coefficient for spontaneous emission, $N(\mathrm{X}_j^{+k})/N(\mathrm{X}^{+k})$ is the relative j-level population of ion X^{+k}, $N(\mathrm{X}^{+k})/N(\mathrm{X})$ is the relative ion population, $N(\mathrm{X})/N(\mathrm{H})$ is the

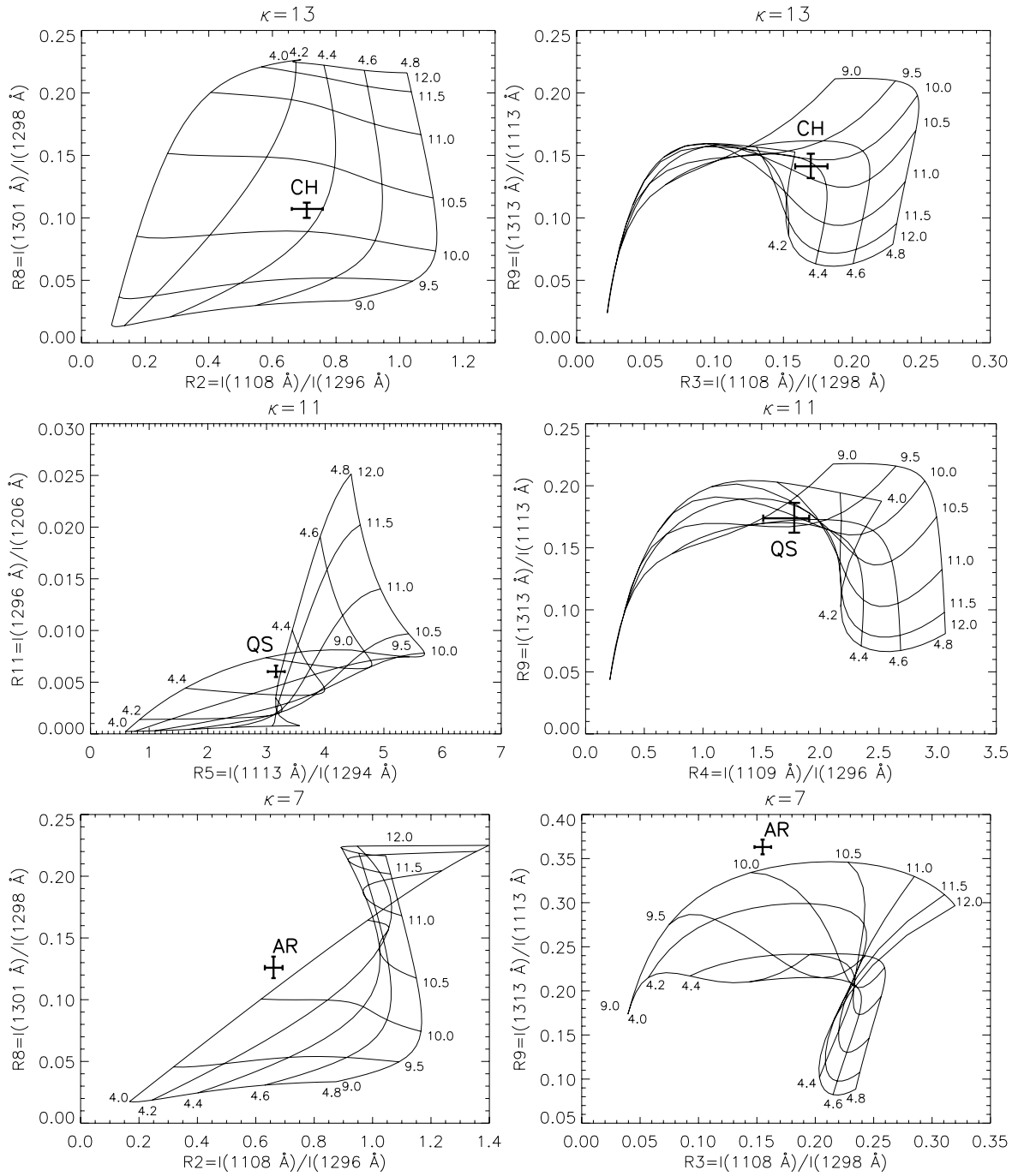

Fig. 6. Resulting diagnostic plots for CH (*top*), QS (*middle*), and AR (*bottom*). The diagnosed parameters T, N_e, and κ are summarized in the Table 3.

abundance of element X relative to hydrogen, $N(\mathrm{H})/N_e$ is the abundance of hydrogen relative to the electron density.

Sets of synthetic spectra for selected DEMs for the Maxwellian distribution and the κ-distributions with the different κ were calculated. We assumed that κ is constant over the transition region in our calculations. This is a simplified assumption because the value of κ should increase and a deviation of a non-thermal distribution from Maxwellian one should decrease toward the chromosphere in the real transition region. We also assume that the atmosphere has a constant pressure that corresponds to $N_e \times T = 10^{13}$–10^{16} cm^{-3} K.

6.1. Contributions to the line intensity

We calculated the contribution to the total line intensity as a function of $\log(T/\mathrm{K})$ to determine the region of T where the spectral lines are formed. We selected lines that correspond to the ratios R2, R9, and R11 to show a typical behavior of Si III lines. The results for the Maxwellian distribution are shown in Fig. 8 *left* and *middle*. Evidently, that there is not a sharp peak that corresponds to a single T, instead a plateau and the spectral lines are formed in a wider range of T, typically from $\log(T/\mathrm{K}) \sim 4.3$ to $\log(T/\mathrm{K}) \sim 4.8$. The character of this plateau depends on the shape of DEM and can be different for different lines. Very strong gradients of DEM in the region of $\log(T/\mathrm{K}) \sim$ 4.0–4.2 can shift the maximum of the contribution to the line intensity to

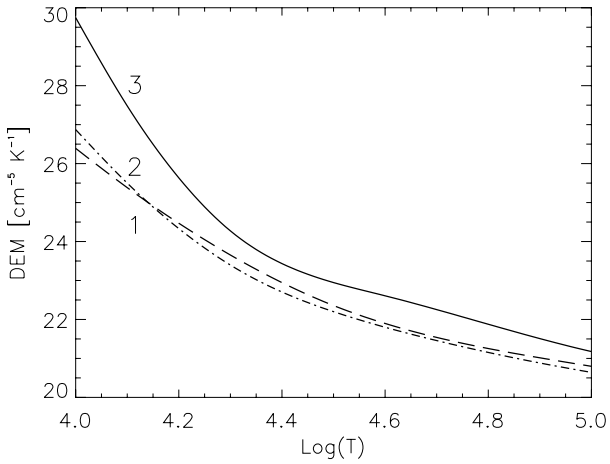

Fig. 7. Dependence of DEM 1 (dashed line), DEM 2 (dot-dashed line), and DEM 3 (full line) on log(T).

log(T/K) ~ 4.0 (Fig. 8, *middle*) for some lines, e.g. 1206, 1296, 1296, and 1108 Å influencing the observed values of their ratios (e.g. $R2$ = 1108/1296, R11 = 1296/1206). These ratios can correspond to log(T/K) ~ 4.0 in some cases if the Maxwellian distribution is assumed. This is very important for the diagnostics of the transition region. It is evident from Fig. 8 that each of the diagnosed plasma parameters is weighted by DEM, and averaged over a wide temperature range of atmosphere.

The results for the κ-distributions show a similar behavior of spectral lines as for the Maxwellian distribution (Fig. 8 right). However, the plateau is wider, the contributions from regions with lower T are higher, and the behavior of various lines becomes similar if a deviation of κ-distribution from Maxwellian distribution increases. Each of the Si III lines shows a maximum of the contribution to the line intensity at $T = 10^4$ K. We must point out that the real contributions to line intensity in the $T \approx 10^4$ K region should be lower than our calculations for the κ-distributions and must be similar to the calculation for Maxwellian distribution owing to Maxwellian boundary condition. We note that the ratio $R9$ = 1313/1113 used for its diagnostics is almost independent from T and DEM. Therefore, the diagnosed value of κ are expected to be correct.

6.2. Line ratios for different DEMs

The calculated line ratios for the Maxwellian distribution and for different DEMs with different pressures in the transition region corresponding to log($N_e \times T$/cm^{-3} K) = 13.0–16.0 are shown in Fig. 9 together with the diagnostic plots and observed line ratios. It is evident from Fig. 9 (top left) that the diagnosed T should be nearly constant for any pressure and DEMs with low gradient. A stronger gradient of DEM shifts the calculated line ratios toward lower T with the pressure remaining approximately constant. On the other hand, the ratio R9, which is very sensitive to the κ-distribution, is placed in the same region for all DEMs (Fig. 9, *right*). The ratio R11 shows a different behavior (Fig. 9 *bottom left*). The ratios calculated in a wide range of pressures are significantly lower than the observed ratios, or ratios predicted by the diagnostic plot. The integration of the 1206 Å line along the line of sight makes the intensity of this line very high. Therefore, the calculated ratios R11 (or R10) for the Maxwellian distributions with any DEMs are much lower than the observed values of these ratios from Pinfield et al. (1999).

Figure 10 shows the comparison of the observed ratios with the calculated ones for different DEMs in atmosphere with diagnosed constant κ and the diagnostic diagrams for this κ. The ratios calculated for different DEMs and log($N_e \times T$) usually correspond to similar values of log($N_e \times T$) from diagnostic diagrams.

The observed and computed ratios for CH agree (Fig. 10, *top*). The observed ratios R2 and R8 correspond to theoretical calculations for the atmosphere with constant log($N_e \times T$/cm^{-3} K) ≈ 14.5 and DEM 1. The ratios R3–R9 give the higher value of log($N_e \times T$/cm^{-3} K) ≈ 14.9–15.0 for DEM 1 or DEM 2. These values are very close to the diagnosed value of log($N_e \times T$/cm^{-3} K) = 14.55 for CH (Table 4). The agreement between the observed ratios for CH with theoretical ones could imply that the real gradient of the DEM in CH is similar to the gradient of DEM 1 by Vernazza & Reeves (1978).

Evidently, that the effect of DEM is able to explain diagnosed $T = 10^4$ K in AR (Fig. 10 *bottom*). The computed points for any DEMs and pressure are close to this T. For the higher gradient of DEM, lower T is obtained. The best result is for the DEM 3. Indeed the observed line ratios correspond to a slightly lower T than 10^4 K, however, CHIANTI does not allow a calculation below this limit. The point corresponding to the observed ratios R2–R8 (R4–R9) is close to the pressure log($N_e \times T$/cm^{-3} K) ≈ 14.1 for DEM 3 that corresponds to the diagnosed value of log($N_e \times T$/cm^{-3} K) = 14.1 (Table 4) for AR.

The explanation of our results with DEM for QS seems to be problematic (Fig. 10 *middle*). On one hand, there is an agreement between our calculations for different DEMs and observed values of R4 and R9. They correspond to DEM with log($N_e \times T$/cm^{-3} K) ≈ 13.9 and the diagnosed value of log($N_e \times T$) is between 13.75–13.8 (Table 4). On the other hand, the point corresponding to the observed ratio R5 and R11 does not correspond to any of the ratios computed for different DEMs and the pressure for the κ-distribution with diagnosed $\kappa \approx 11$ (Fig. 10 *bottom*). The observed value of R11 is much higher than any calculated R11. The shape of DEMs has a small effect only and is not able to reproduce the observed data. The problem could be in the assumption of a constant κ in our calculations. In reality, κ should increase toward the base of the transition region where the electron distribution function should be a Maxwellian one because of its high density. Such changes in κ can result in the shift of our calculations for DEMs to the calculations for the Maxwellian distribution (Fig. 9 bottom left). However, this effect is not completely sufficient to explain the disagreement. Therefore, we assumed that the ratio R11 can be partly influenced by an opacity of the 1206 Å line, although Pinfield et al. (1999) found no flattening of the Gaussian profile of this line in QS. On the other hand, Avrett & Loeser (2008) have pointed out that a line that is strong enough to have its line-center optical depth close to unity in a region where the temperature increases with height, will appear in emission if the line source function also increases with height.

6.3. Optical thickness of the 1206 Å Line

We have to estimate the optical thickness of the 1206 Å line. We have the expression (e.g. Mihalas 1978) to find out the influence of the 1206 Å line opacity on diagnostics

$$\tau_\nu = \frac{B_{ij}}{4\pi} h\nu \int N(\mathrm{X}_i^{+k}) \left(1 - \frac{g_i N(\mathrm{X}_j^{+k})}{g_j N(\mathrm{X}_i^{k})}\right) \Phi(\nu) \mathrm{d}l, \quad (3)$$

where B_{ij} is Einstein coefficient for absorption, $\Phi(\nu)$ is an absorption profile, $N(\mathrm{X}_i^{+k})$, and $N(\mathrm{X}_j^{+k})$ are the density of a k-times

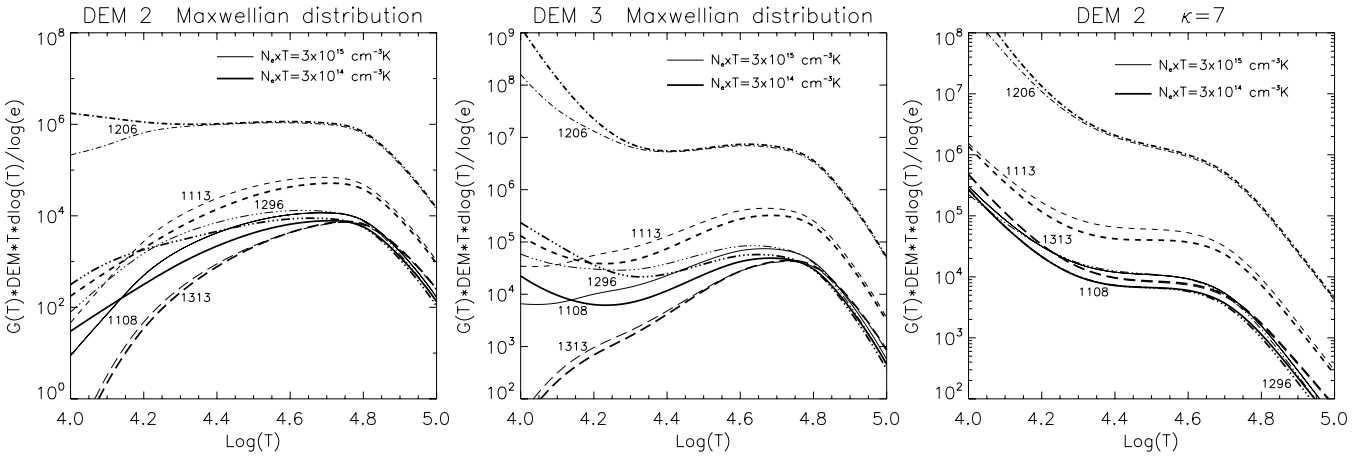

Fig. 8. Contributions to the total intensity of Si III lines 1108, 1296, 1313, 1113, 1296, and 1206 Å as a function of $\log(T/\mathrm{K})$ computed for the solar atmosphere with the Maxwellian distribution electrons with DEM 2 (*left*) and DEM 3 (*middle*), and the κ-distribution with $\kappa = 7$ and DEM 3 (*right*). Thin lines correspond to the constant pressure $N_e \times T = 3 \times 10^{15}$ cm^{-3} K and thick lines are for 3×10^{14} cm^{-3} K.

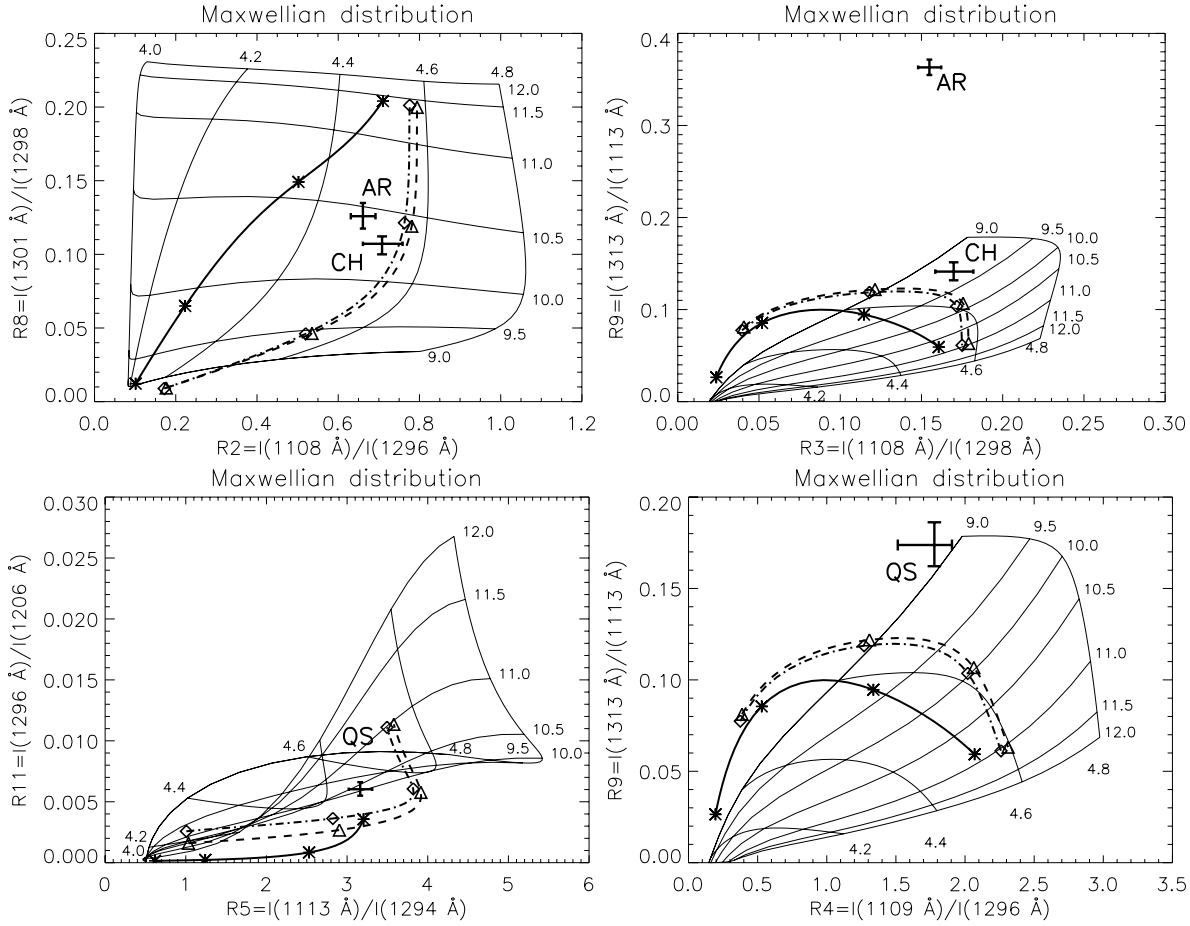

Fig. 9. Relation between ratios R2 and R8 (above, *left*), R3–R9 (above, *right*), R5–R11 (below, *left*) and R4–R9 (below, *right*) for the Maxwellian distribution (thick black lines) computed for the solar atmosphere with a constant pressure characterized by $N_e \times T = 10^{13}$–10^{16} cm^{-3} K with the DEM 3 (full lines), DEM 2 (dot-dashed lines), and DEM 1 (dashed lines). The points correspond to DEMs with $N_e \times T = 10^{13}$, 10^{14}, 10^{15}, and 10^{16} cm^{-3} K. The crosses with error bars show observed line ratios.

Table 4. Comparison of the diagnosed $N_e \times T$ with pressure estimated for different DEMs.

	$\log(N_e \times T / \mathrm{cm}^{-3}\,\mathrm{K})$		
	Coronal hole	Quiet Sun	Active region
Diagnosed from T and N_e	14.55	13.75–13.80	14.1
Estimated from DEM	14.50–15.00	13.90*	14.1

Notes. (*) From R4–R9 only.

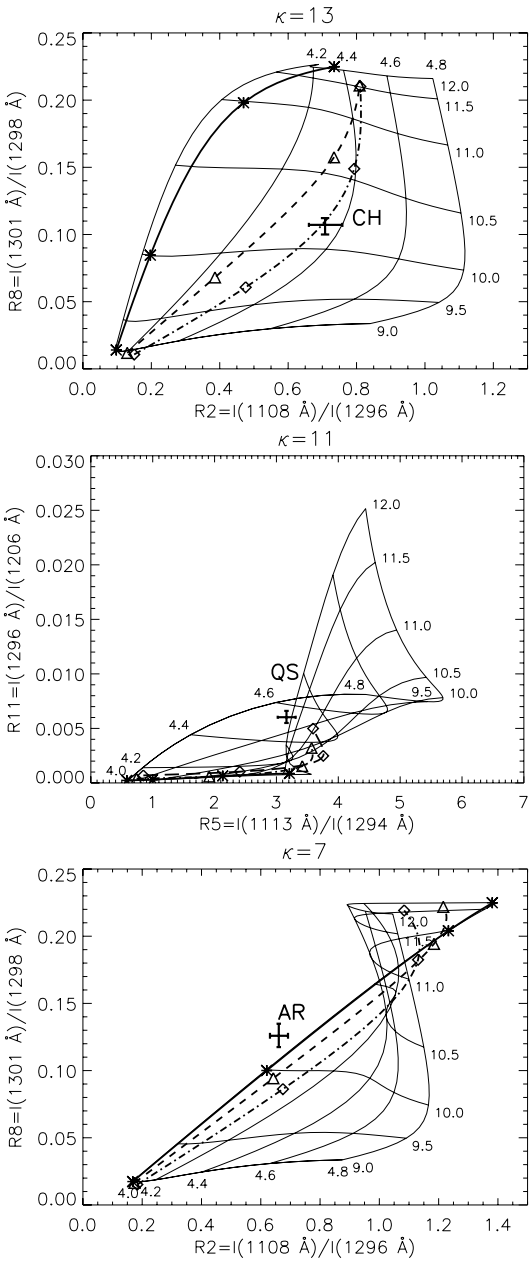

Fig. 10. Comparison of the calculated R2–R8 for different DEMs (DEM 1: dashed line, DEM 2: dot-dashed line, DEM 3: full line) and $\kappa = 13$ with the diagnostics figure for $\kappa = 13$ (*top*), calculated R5–R11 for different DEMs and $\kappa = 11$ with the diagnostics figure for $\kappa = 11$ (*middle*), and calculated R2–R8 for different DEMs and $\kappa = 7$ with the diagnostics figure for $\kappa = 7$ (*bottom*). The black crosses with the error bars mark observed line ratios in CH, QS, and AR.

ionized atom with excited level i, and j, respectively, g_i and g_j are statistical weight of the levels i and j. The term in a brackets is the correction for the stimulated emission. The absorption profile in the transition region can be approximated by the thermal Doppler profile

$$\Phi(\nu) = \frac{1}{\sqrt{\pi}\Delta\nu_{\rm D}} \exp\left(-\frac{(\nu-\nu_0)^2}{\Delta\nu_{\rm D}^2}\right), \quad (4)$$

where $\Delta\nu_{\rm D} = (\nu_0/c)(2kT/M)^{1/2}$ is the Doppler line width and M is the mass of the element. Finally, the optical thickness in a line

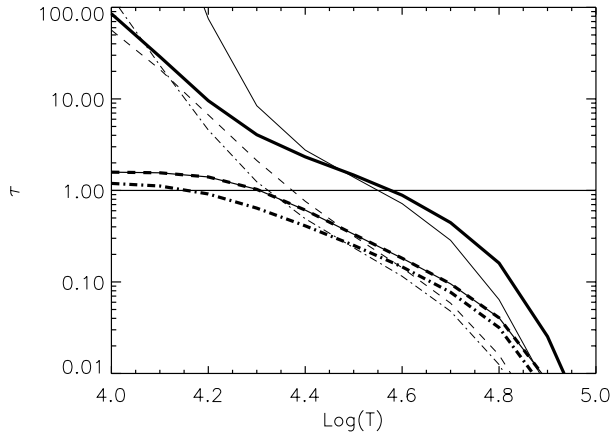

Fig. 11. Optical thickness in center of the 1206 Å line for different DEMs (DEM 1 – dashed lines, DEM 2 – dot-dashed lines, DEM 3 – full lines), for the Maxwellian distribution (thick lines) and κ-distribution with $\kappa = 12$ (thin lines).

center ($\nu = \nu_0$) is

$$\tau_{\nu=\nu_0} = \frac{B_{ij}}{4\pi^{3/2}}\frac{h\nu}{\Delta\nu_{\rm D}}\int\left(1-\frac{g_i N(\mathrm{X}_j^{+k})}{g_j N(\mathrm{X}_i^{+k})}\right)\frac{N(\mathrm{X}_i^{+k})}{N(\mathrm{X}^{+k})}\frac{N(\mathrm{X}^{+k})}{N(\mathrm{X})} \times \frac{N(\mathrm{X})}{N(\mathrm{H})}\frac{N(\mathrm{H})}{N_{\rm e}}\frac{1}{N_{\rm e}}\mathrm{DEM}\,\mathrm{d}T. \quad (5)$$

The dependence of the calculated optical depth for the 1206 Å line center for atmospheres with different DEMs and for Maxwellian and κ-distributions with $\kappa = 12$ are in Fig. 11. The calculated τ reaches value $\tau = 1$ (marked by full line) for $T_{\tau=1} \approx 10^{4.2}$–$10^{4.6}$ K for each of DEM and the distributions. The real value of $T_{\tau=1}$ mainly depends on the shape of DEM. The κ-distribution significantly increases the optical depth of 1206 Å line for low T because it increases the Si III abundance in this region of T. We do not know the real DEM in the observed region but there is a high probability that the optical depth in the center of this line is higher than 1. The radiative transfer in this line must be calculated to solve this problem. Our calculations show that this line is inappropriate for diagnostics.

We can conclude that the values of $\log(N_{\rm e})$ and $\log(T)$ in Table 3 agree with $\log(N_{\rm e} \times T)$ derived for the atmospheres with different DEMs. This means that the strong T and density gradients in the transition region have little effect on the diagnosed value of κ. The strong gradient of DEM can influence the diagnosed value of T and $N_{\rm e}$ but their product (pressure) seems to be correct. Therefore, the influence of DEM on the line ratios can explain the very low T value diagnosed in AR with low κ, The results for QS could be influnced by the optical thickness of the 1206 Å line, however, the diagnosed κ should be correct.

7. Conclusion

The diagnostic method for the parameters κ and T and the electron density from observed intensity ratios of Si III lines have been proposed in this paper. We included the radiation field in our calculation of the thermal and non-thermal excitation equilibrium. We demonstrated that the observed line ratios can be explained by the presence of the non-thermal electron κ-distributions in the transition region. The agreement between the theoretical line ratios for the non-thermal κ-distributions and the observations provides evidence for the presence of the κ-distributions or very similar ones in the transition region.

The results showed that only a slightly higher degree of non-thermality is diagnosed in the QS region ($\kappa \approx 11$) than in CH with $\kappa \approx 13$. The electron distribution in AR shows the strongest deviation from the Maxwellian distribution with $\kappa = 7$. This means that the region with an intensified magnetic field can enhance the suprathermal tail of the distribution. The diagnosed values of N_e correspond to the typical parameters of plasma in the transition region. The values of T for the κ-distributions with a higher κ are close to the temperatures from the Maxwellian diagnostics. The low T value diagnosed in AR with the highest degree of non-thermality can be a result of the influence of DEM on the observed line ratio. The effect of DEM is able to explain some peculiarities in the diagnosed plasma parameters. Low values of the ratios R10 and R11 compared with observations can be an effect of optical thickness of the 1206 Å line, which we do not recommend for diagnostics. The results can be influenced by existing plasma inhomogeneities or variations of κ within the transition region.

Acknowledgements. This work has been supported by Grant No. 205/09/1705 of the Grant Agency of the Czech Republic, grant No. 1/0240/11 of Scientific Grant Agency VEGA, Slovakia, and ESA-PECS project No. 98030. We used the CHIANTI software and database. CHIANTI is a collaborative project involving the NRL (USA), RAL (UK), MSSL (UK), the Universities of Florence (Italy) and Cambridge (UK), and George Mason University (USA).

References

Avrett, E. H., & Loeser, R. 2008, ApJS, 175, 229
Baluja, K. L., & Hibbert, A. 1980, J. Phys. B, 13, L327
Dere, K. P., Landi, E., Young, P. R., et al. 2009, A&A, 498, 915
Doschek, G. A., Feldman, U., Laming, J. M., et al. 1998, ApJ, 507, 991
Dufton, P. L., & Kingston, A. E. 1989, MNRAS, 241, 209
Dufton, P. L., Hibbert, A., Kingstone, A. E., & Doshek, G. A. 1983, ApJ, 274, 420
Dufton, P. L., Kingston, A. E., & Keenan, F. P. 1984a, ApJ, 280, L35
Dufton, P. L., Keenan, F. P., & Kingston, A. E. 1984b, MNRAS, 209, 1P
Dzifčáková, E. 1992, Sol. Phys., 140, 247
Dzifčáková, E. 2002, Sol. Phys., 208, 91
Dzifčáková, E. 2005, Sol. Phys., 234, 243
Dzifčáková, E. 2006, Proc. of SoHO-17: 10 Years of SoHO and Beyond, 7–12 May, Giardini Naxos, Sicily, Italy, ed. H. Lacoste, & L. Ouwehand, ESA SP-617, 89.1
Dzifčáková, E., & Mason, H. 2008, Sol. Phys., 247, 301
Keenan, F. P., & Kingston, A. E. 1986, MNRAS, 220, 493
Keenan, F. P., Cook, J. W., Dufton, P. L., & Kingston, A. E. 1989a, ApJ, 340, 1135
Keenan, F. P., Dufton, P. L., & Kingston, A. E. 1989b, Sol. Phys., 123, 33
Landi, E., Del Zanna, G., Young, P. R., et al. 2006, ApJS, 162, 261
Ljepojevic, N. N. 1988, J. Quant. Spect. Rad. Transfer, 44, 203
Ljepojevic, N. N., & MacNeice, P. 1988, Sol. Phys., 117, 123
MacNeice, P., Fontenla, J., & Ljepojevic, N. N. 1991, ApJ, 369, 544
Maksimovic, M., Pierrard, V., & Riley, P. 1997, Geophys. Res. Lett., 24, 1151
Martin, W. C., Sugar, J., Musgrove, A., & Dalton, G. R. 1995, NIST Database for Atomic Spectroscopy, Version 1.0, NIST Standard Reference Database 61
Mihalas, D. 1978, Stelar Atmosphere (San Francisco: W. H. Freeman, & Co.)
Nieves-Chinchilla, T., & Viñas, A. F. 2008, J. Geophys. Res., 113, A02105
Owocki, S. P., & Scudder, J. D. 1983, ApJ, 270, 758
Pérez, M. E., Doyle, J. G., O'Shea, E., & Keenan, F. P. 1999, ApJ, 351, 1139
Philips, K. J. H., Feldman U., & Landi, E. 2008, Ultraviolet and X-ray Spectroscopy of the Solar Atmosphere (New York: Cambridge University press)
Pierrard, V., & Lazar, M. 2010, Sol. Phys., 267, 153
Pinfield, D. J., Keenan, F. P., Mathioudakis, M., et al. 1999, ApJ, 527, 1000
Roussel-Dupré, R. 1980, Sol. Phys., 68, 265
Scudder, J. D. 1992, ApJ, 398, 349
Scudder, J. D., & Olbert, S. 1978a, J. Geophys. Res., 84, 2755
Scudder, J. D., & Olbert, S. 1978b, J. Geophys. Res., 84, 6603
Shoub, E. C. 1983, ApJ, 266, 339
Vernazza, J. E., & Reeves, E. M. 1978, ApJS, 37, 485
Vocks, C., Mann, G., & Rausche, G. 2008, A&A, 480, 527
Wannawichian, S., Ruffolo, D., Kartavykh, & Yu. Yu. 2003, ApJS, 146, 443
Zouganelis, I. 2008 J. Geophys. Res., 113, 8111